Arabian Journal of Chemistry (2020) 13, 1229–1246

King Saud University

Arabian Journal of Chemistry

www.ksu.edu.sa
www.sciencedirect.com

ORIGINAL ARTICLE

Structural, morphological, optical and sensing properties of SnSe and $SnSe_2$ thin films as a gas sensing material

Kawther Assili [a,b,*], Oriol Gonzalez [b], Khaled Alouani [a], Xavier Vilanova [b]

[a] University of Tunis El Manar, Faculty of Science, Laboratory of Analytical Chemistry and Electrochemistry, Campus, 2092 Tunis, Tunisia
[b] University Rovira i Virgili, Department of Electronic, Electrical and Automatic Engineering, 43007 Tarragona, Spain

Received 11 July 2017; accepted 22 October 2017
Available online 28 October 2017

KEYWORDS

Triphenylphosphine selenide;
CVD;
SnSe thin film;
XRD;
Optical properties;
Sensing properties

Abstract In this work, orthorhombic tin selenide thin films were grown onto three different substrates using an organophosphorus precursor (Ph_3PSe) via chemical vapor deposition. Structural, microstructural and morphological properties of the as-grown films were systematically investigated using XRD, ESEM and AFM respectively. Grain size, microstrain and dislocation were calculated and correlated with different factors. The effects of selenization temperature and substrate type on different film properties and gas sensing response of films deposited onto alumina substrates were investigated. XRD analysis reveals the appearance of a mixed phase as a function of temperature. Furthermore, substrate type plays a key role in the rate of appearance of each phase. EDAX analysis confirms the existence of the desired elements and detect the evaporation of selenium and the appearance of oxygen at higher temperatures. Atomic force microscopy (AFM) was used to investigate the surface topography of the grown thin films.

Optical properties of the films grown onto glass and silicon substrates were studied. From the recorded optical data, a direct optical band gap in the range of 0.9–1.3 eV was obtained with an absorption coefficient $\alpha > 10^4\ cm^{-1}$ throughout large spectral regions. Optical studies were remarkably affected by the obtained phase as well as the selenization temperature. Gas sensing properties of the samples deposited onto alumina substrates were examined as a new sensing material for detection of methane gas at different concentrations. SnSe sensors show high sensitivity, are reversible and exhibit fast response and recovery times compared to $SnSe_2$ sensors.

* Corresponding author.
E-mail address: kawther.assili@fst.utm.tn (K. Assili).
Peer review under responsibility of King Saud University.

Production and hosting by Elsevier

1. Introduction

Finding suitable precursors with high efficiency and good performance is one of main challenges in the semiconductor field, since many requirements should be accounted for when mak-

https://doi.org/10.1016/j.arabjc.2017.10.004
1878-5352

ing a selection (e.g., abundancy, manufacturing cost, stability and environmental effect). Whereas, several attempts to prepare binary semiconductors with various metal-series such as Sb (I), Pb (II), In(III), and Sn (II) had been successful using conventional chalcogenide precursors such as thiourea SC $(NH_2)_2$, thioacetamide C_2H_5NS, selenourea $(SeC(NH_2)_2)$, Na_2SeSO_3, $TeCl_4$, Na_2TeO_3.

Nowadays, the use of organo- phosphinato-chalcogeno-compounds as a precursor presents a new way for thin film deposition. It leads to the formation of a variety of metal chalcogenide as ZnS (Opoku et al., 2015), NiS (Panneerselvam et al., 2010), SnS (Assili et al., 2017), InSe (Afzaal et al., 2005; Park et al., 2003), Bi_2Se_3 (Waters et al., 2003), CdSe (Afzaal et al., 2002), ZnSe (Afzaal et al., 2002), Ni_xSe (Panneerselvam et al., 2008), Ge_2Te_3 (Garje et al., 2006); In_2Te_3 (Waters et al., 2003), HgTe (Briand et al., 2002; Chivers et al., 2005).

Among this various binary metal-chalcogenide materials, Tin selenide, SnSe, with its different forms, crystal bulk and thin films has been extensively studied from several points of view: experimental, applied and even fundamental investigation (Kim et al., 2016). The success key of this material is mainly related to its potential physical properties (optical and electrical), which fulfil the essential requirements of several structures (Guan et al., 2015; Singh et al., 2016), and technological applications (Baumgardner et al., 2010; Pejova and Tanuševski, 2008). SnSe is a member of IVA-VIA binary semiconductors family, with high absorption coefficient (He et al., 2013), narrow optical band gap (Shi and Kioupakis, 2015) (range from 0.9 to 1.3 eV for both direct and indirect band gaps respectively) and exhibits p or n-type conduction (Shi and Kioupakis, 2015; Anwar et al., 2015). Recently, many investigators have proven that it could be a good prospective photoelectric and thermoelectric material thanks to its interesting thermoelectric behavior (Ferreiro et al., 2017; Anwar et al., 2016). Heremans has shown that SnSe has a high Carnot efficiency for a thermoelectric cycle (Heremans, 2014). In a recent report, Zhang et al. has declared that SnSe possess unexpectedly low thermal conductivity in the world (Zhang and Talapin, 2014). Furthermore, the higher anharmonicity of chemical bonds in the SnSe structure has resulted in interesting photon transport properties, thus a weird anisotropic properties (Xu et al., 2017).

Besides all these exotic physical properties, SnSe, is an abundant, stable, and low production cost material with superconductivite properties (Timofeev et al., 1997) and a strong power factor (Zhao et al., 2016) that boost it's photoelectric and thermoelectric efficiency.

All these characteristics can justify the classification of tin selenides among the most promising semiconductors and allows it's application in several electronic and optical devices as light emitting devices (Kumar et al., 2015), anode laser material (Ning et al., 2011; Zainala et al., 2004), photoelectrical cells (Mathews, 2012), sensors (Popescu et al., 2007), anode material for rechargeable lithium batteries (Xue et al., 2006), memory switching devices (Chung et al., 2008), only to cite a few.

In fact, there are numerous methods for the preparation of tin selenide thin films, such as spray pyrolysis (Anwar et al., 2015), electrodeposition (Subramanian et al., 1999), thermal evaporation (Indirajith et al., 2010), chemical bath deposition (CBD) (Zainal et al., 2004), and chemical vapor deposition (CVD) (Butt et al., 2014). However, in the last few years, the interest in the latter has grown enormously, due to its advantages of suitability to deposit different materials with good quality, high adhesion and overall simplicity.

As our own work on thin solid film consists of testing the suitability of some organophosphorus precursors for depositing metal chalcogenide thin films, a previous attempt has successfully lead to deposit SnS thin films using the molecule $Ph_3P = S$ as a sulfur precursor. Moreover, as SnSe is an analogue of SnS from the point of view of structural properties, the present attempt consists of probing the performance of the triphenylphosphine selenide (Ph_3PSe) as an alternative selenide precursor in order to deposit tin selenide thin films using a low cost technique. On the other hand, the deposition of SnSe using Ph_3PSe as a precursor can avoid the formation of toxic products such as H_2Se, since the by-product in this attempt is the stable molecule Ph_3P or the main precursor Ph_3-PSe, that are more ecofriendly than other precursor and processes. It is important to consider that until now; no thin film material had been deposited using this compound.

In the present work, a detailed investigation on the chemical vapor deposition (CVD) of tin selenide thin films using triphenylphosphine selenide was reported. Furthermore, the results obtained until the moment indicate that, the structural optical and electrical properties of materials can be influenced by the process conditions and methods used in their deposition. Indeed, it is crucial to study the effect of substrate type and selenization temperature on the properties of the film deposited. Glass, silicon and alumina are the different types of substrates that were used to deposit tin selenide thin films in a temperature range from 200 °C to 500 °C. The study of the selenization temperature and substrate type influence on the microstructure and morphology of the resulting tin selenide thin films is performed by XRD, EDAX, SEM and AFM. The optical properties of the SnSe films deposited onto glass and silicon substrates were obtained. The gas sensing properties of the SnSe films deposited onto alumina were tested as a sensor material for detection of methane gas. This sensing capability has been reported previously (Popescu et al., 2007), although, the sensing layer was, in fact, a mixture on $SnSe_2$ and SnO_2, since the sensor was operated over 500 °C, which produces the oxidation of the layer. The SnSe (nanosheets) and SnO_2 (nanoparticles) combination has been also reported as gas sensor by Wang et al., 2013.

2. Deposition and characterization of thin films

2.1. Precursor preparation

For the deposition of tin selenide thin films, triphenylphosphine selenide has been synthetized by reaction between triphenylphosphine and an equivalent amount of selenium powder in anhydrous acetonitrile. The reaction mixture was stirred for 8 h at −10 °C. After filtration and evaporation of the solvent, the desired compound was obtained after recrystallization from absolute ethanol, mp 187–188 °C.

2.2. Substrate preparation

The cleaning procedure of the glass microscope slides substrate (dimension 1.2 × 1 cm × 1.2 mm), can be found elsewhere

(Assili et al., 2017). The silicon substrates Si (1 1 1) (dimension 1 × 1 cm × 0.025 mm) were rinsed in distilled water, acetone, methanol and ethylene glycol respectively. Prior to film preparation, the native oxide of the silicon wafers was removed by dipping the substrates in 20% HF solution and washing them in distilled water and ethanol. On the other hand, the alumina substrates were used without previous cleaning.

2.3. Film deposition

Two simple steps were used to deposit tin selenide thin films onto different substrates. The process involves the deposition of a tin layer with a 100 nm thickness by a sputter deposition process. A two-inches Sn target (99.99% pure) was used and placed at a substrate distance of 35 mm. The DC sputtering power was set to 200 W and the deposition process was performed during 720 s, at 3 mTorr of vacuum pressure in a 120 sccm flow of Argon. This operation was followed by the selenization of the tin layer as a second step (Fig. 1).

The selenization process occurs during 90 min via a normal chemical vapor deposition using 0.01 g of triphenylphosphine selenide, which allows the formation of SnSe thin films. The selenization process was carried out in the presence of argon onto three different types of substrates and at a temperature (T_{sel}) that ranged from 200 °C to 500 °C at 100 °C steps. All tin selenide samples were operated using the CVD condition described in our previous paper (Assili et al., 2017).

2.4. Film characterization

XRD measurements were made using a Bruker-AXS D8-Discover diffractometer equipped with parallel incident beam (Göbel mirror), vertical θ-θ goniometer, XYZ motorized stage and with a GADDS (General Area Diffraction System). Samples were placed directly on the sample holder for reflection analysis. An X-ray collimator system close-to-the-sample allows to analyze areas of 500 μm. The X-ray diffractometer was operated at 40 kV and 40 mA to generate Cu kα radiation. The GADDS detector was a HI-STAR (multiwire proportional counter of 30 × 30 cm with a 1024 × 1024 pixel) placed at 15 cm from the sample. We collected three frames (2D XRD pattern) that covered at such distance a range from 20 up to 89° 2θ. The exposition time was of 300 s per frame. The analysis were done in Bragg-Brentano condition. The resulting images were 2θ integrated to obtain a 2θ conventional diffractogram. Identification of the minerals was achieved by comparison of the XRD diffractogram with the ICDD data base (release 2007) using Diffracplus Evaluation software (Bruker 2007). The surface morphology and the atomic composition were determined using environmental scanning electron Quanta 600 microscope from FEI Company. The surface topology of the films deposited were investigated using atomic force microscopy (AFM) type Keysight Model 5500, using acoustic mode (tapping mode), with a tip of 300 kHz and 75 kHz resonance frequency for 5 × 5 μm^2 area.

Using VARIAN spectrophotometer, the optical transmittance and reflectance of the samples were measured within the wavelength range of 250–2500 nm at room temperature. For the measurement of the transmission of SnSe films on Si, a silicon substrate was used as a reference in order to decouple the absorption of the film from that of the substrate.

2.5. Sensor measurement

For the gas detection tests, the sensor devices were placed in a sealed Teflon chamber equipped with appropriate inlet and outlet for gas. The different materials were deposited onto an alumina substrate having a pair of comb like platinum electrodes on one side and a platinum heater on the other side. Fig. 2 shows the picture of the used chamber containing the sensors. The gas sensing measurements started by heating the sensors using DC power supply until stabilization of their baseline resistance. After that, methane gas diluted in dry air was injected into the chamber at different concentrations

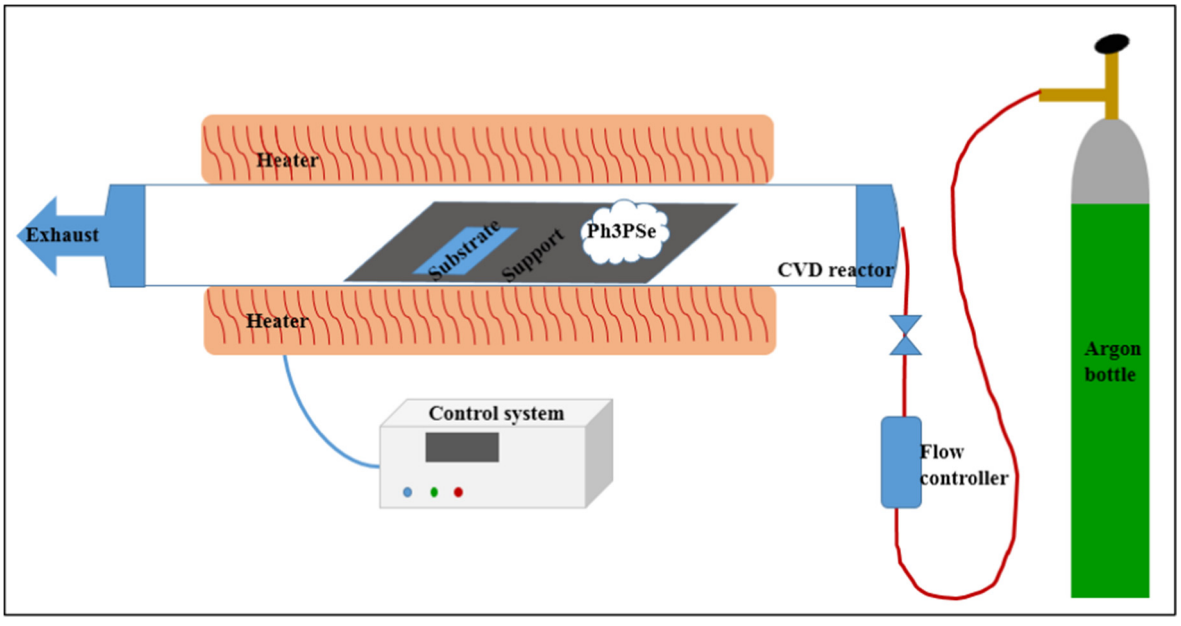

Fig. 1 Schematic illustration of the experimental system.

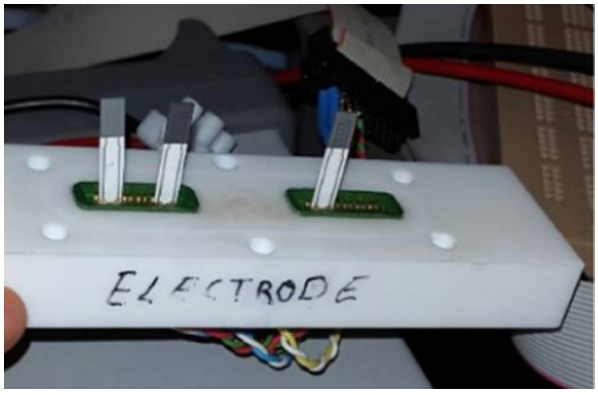

Fig. 2 Picture of the test chamber containing three sensors.

(0.2%, 0.5% and 1%) by means of computer driven mass follow controllers.

Sensor response (R) was defined as:

$$R = \frac{R_a - R_g}{R_a} \times 100\%$$

where R_a and R_g are the electrical resistance of the sensor exposed to air and to methane diluted in air, respectively.

The response time was defined as the time taken by the sensors to reach 90% of the total resistance change upon exposing the sensor to methane gas, while recovery time was defined as the time recorded to recover 90% of the initial resistance (Lou et al., 2013).

3. Results and discussion

3.1. Crystallinity

XRD technique was used to check the different phases existing onto the films. The structural identification of different phases has been carried out in an angular range $20 \leq 2\theta \leq 89$ (Fig. 2). The growth involves the reaction of tin with the free selenide ions obtained following the thermal decomposition of Ph_3PSe. Figs. 3a–3c corresponds to the typical XRD patterns of films prepared onto glass, silicon and alumina respectively for different selenization temperatures. It is clear from the different XRD patterns that all diffractograms contain intense and sharp peaks, which reflects the good crystalline quality and assures the correct nature of the films obtained. All samples deposited show the presence of several reflections, matching well with the Joint Committee on Powder Diffraction Standard (JCPDS) data (File No. 048-1224) of the orthorhombic structure of SnSe (Boudjouk et al., 1996). It is also clearly observed that all samples, besides those deposited onto alumina substrate, present common intense diffraction peaks at $2\theta = 30.5°$. For the films deposited onto alumina, the same peak was observed, but with lower intensity, as the highest was related to the substrate diffraction. For different substrate types and for all the range of temperatures studied, the preferred orientation corresponds to the (1 1 1) plane, located at $2\theta \approx 30, 5°$. Therefore, it is found that no matter the type of the substrate used, regardless glass, silicon or alumina, SnSe deposited by CVD method-using Ph_3PSe crystallizes in orthorhombic structure. Other peaks corresponding to the (2 0 1), (0 1 1), (3 1 1), (1 0 2), (4 1 1), (3 0 2), (5 1 1), and (4 2 0) reflections of the SnSe orthorhombic were also observed. Furthermore, other less intense peaks were also detected, differing from one sample to another, depending on the selenization temperature or substrate type, but with notably lower intensities.

Biçer and Sisman (2011) also found the same preferred orientation along (1 1 1) plane for SnSe films deposited by electrodeposition. However, Indirajith et al. (2010) observed a preferred orientation along (4 0 0) for SnSe films prepared by thermal evaporation technique. Other preferred orientation along (2 1 0) and (4 0 2) planes were observed for SnSe thin films deposited by electrodeposition (Subramanian et al., 1999). This analysis reveals that the deposition method plays a crucial role in the structural properties of the films. However, in our case, the existence of the same preferred orientation for all the deposited films indicates that the nature of the substrate and the temperature plays no role in the growth orientation of the grain.

From the XRD patterns presented in Figs. 3, it is clear that all the films are polycristalline in nature, regardless of selenization temperature or substrate type. The X-ray diffraction patterns of the films deposited onto glass substrate (Fig. 3a.) show that at lower temperature only SnSe phase was formed; however, when the temperature raises up to 300 °C the peak intensities start to increase and some new peaks related to the hexagonal $SnSe_2$ phases appear (card no. 01-089-2939), with space group P_{-3m1} (Busch et al., 1961). Moreover, this observation can indicate that temperatures lower than 300 °C were too low to form the $SnSe_2$ phase. This second tin selenide phase disappears with further increasing the selenization temperature up to 400 °C, where only SnSe phase remains, but with decreasing peak intensity. When the selenization temperature was further increased to 500 °C, a tetragonal oxide phase SnO_2 (card no. 00-041-1445) (McCarthy and Welton, 1989) appear simultaneously with the SnSe phase. On the other hand, the samples formed by pure SnSe phase show the best crystalline nature.

For a similar deposition, Fernandes et al. have obtained a hexagonal $SnSe_2$ onto glass substrate for a temperature range from 300 to 470 °C, and after a dissociation processes, SnSe appear at higher temperature (530–570 °C) (Fernandes et al., 2013). The appearance of $SnSe_2$ starting at 300 °C is in accordance with our results, while the difference in SnSe formation temperature can be attributed to the difference in physical properties of the precursor.

For the samples deposited onto silicon substrates, it is found that deposition at 200 °C for 90 min leads to poor material formation. This can be derived from the XRD patterns (Fig. 3b) by the presence of some peaks corresponding to tin (card no. 00-004-0673) (Tatge, 1953) along with SnSe peaks. Thereby, this indicates that this lower temperature cannot allow the reaction of all the tin present. By increasing the temperature above 200 °C, the peak related to Sn disappears and peaks associated to SnSe and $SnSe_2$ have been recorded in the XRD, showing a better crystallinity. Finally, it is found that at the selenization temperature of 500 °C leads to the formation of pure SnSe phase with well-crystallized films.

Differently, the XRD patterns of the films deposited onto alumina substrate show the presence of higher intensity peaks, related to the substrate, along with those of SnSe phases and

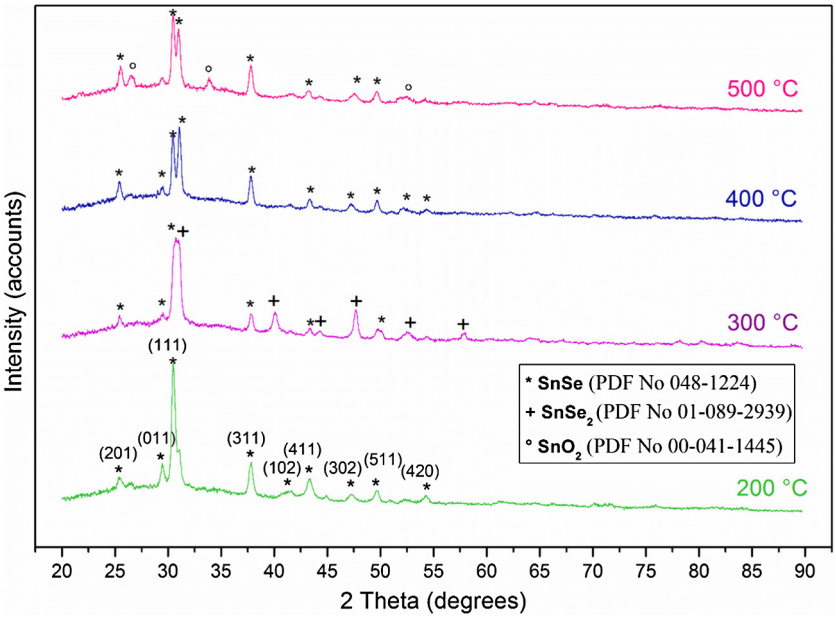

Fig. 3a X-ray diffraction patterns of SnSe films deposited onto glass substrates for the different selenization temperatures.

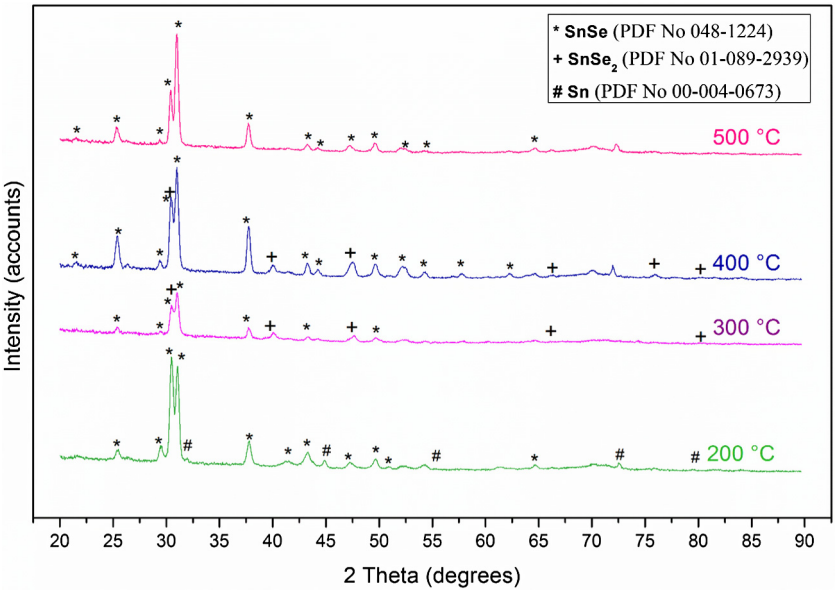

Fig. 3b X-ray diffraction patterns of SnSe films deposited onto silicon substrates for the different selenization temperatures.

other secondary phases present, depending on the selenization temperature used. Moreover, when the selenization temperature increases from 200 °C to 300 °C, the obtained phase changes from SnSe to pure $SnSe_2$, but when reaching 400 °C, SnSe appears again and $SnSe_2$ completely disappears. This fact may be explained by the detachment of some quantity of selenium at higher temperatures. This explanation is further supported by the appearance of the tin oxide phase (SnO_2) together with SnSe. This is caused by the detachment of selenium at higher temperatures, but with replacement of the selenium with oxygen.

The formation of different phases with changing selenization temperature may be summarized in the following way:

Step 1: $2Sn + Ph_3PSe \rightarrow SnSe + Sn + Ph_3P$
Step 2: $SnSe + Sn + Ph_3PSe \rightarrow 2SnSe + Ph_3P$
Step 3: $2SnSe + Ph_3PSe \rightarrow SnSe + SnSe_2 + Ph_3P$
Step 4: $SnSe + SnSe_2 \rightarrow 2SnSe + Se$
Step 5: $2SnSe + O_2 \rightarrow SnO_2 + SnSe + Se$

In fact, the formation of SnSe in the first and second step is the result of the reaction between Sn deposited onto substrate and the Se detached from the Ph_3PSe through the reaction:

$Sn + Se \rightarrow SnSe$ for which the $\Delta H°_{298,f} = -21.5 \pm 1.7$ kcal mol^{-1} (Colin and Drowart, 1964). However, the formation of SnSe in the fourth step can be attributed to a sublimation of $SnSe_2$ through the reaction: $SnSe_2 \rightarrow SnSe + 1/x\ Se_x$

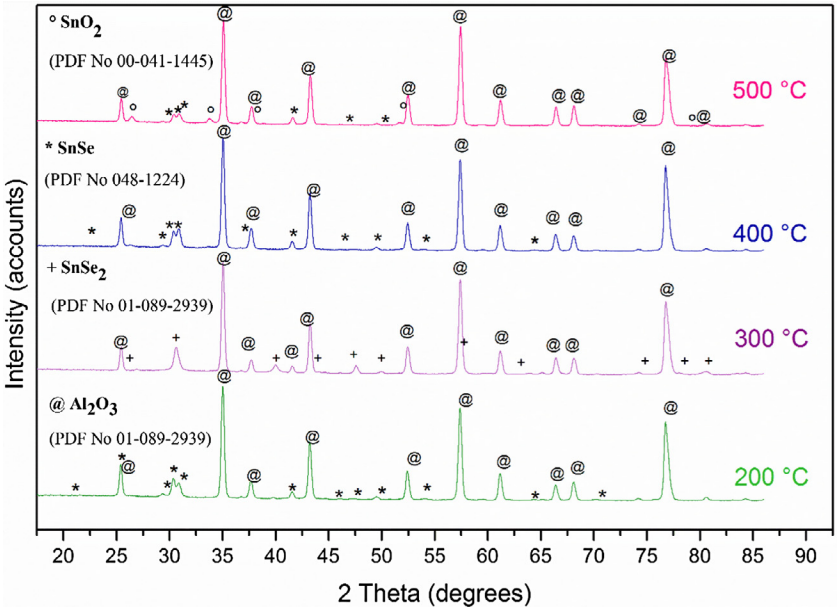

Fig. 3c X-ray diffraction patterns of SnSe films deposited onto alumina substrates for the different selenization temperatures.

being the heat of formation $\Delta H°_{298,f} = -118.1 \pm 15.1$ kJ mol^{-1} (Wieihcmei and Pultz, 1983). On the other hand and based to Se-Sn phase diagram, the formation of $SnSe_2$ needs an atmosphere rich on Se ($50 \leq [Se] \leq 67\%$), while an atmosphere poor on Se ($[Se] \leq 50\%$) allows the formation of SnSe (Sharma and Chang, 1986).

The average crystallite size (D) of the films was determined using FWHM data and Debye-Scherrer approach (Scherrer and Von Der Gesellschaft Der Wissenschaften Zu Göttingen, 1918).

$$D = \frac{k\lambda}{\beta \cos(\theta)} \quad (1)$$

where D is the average diameter of the crystallites, λ is the wavelength of X-ray radiation (Cu K_α), k is the Scherrer constant (0.9), β is the full width at half-maximum intensity of peaks in radians and θ is the Bragg diffraction angle. The crystallite size values estimated from the above formula (1) for different samples are reported in Table 1.

Interestingly, samples deposited onto alumina and glass have the same behavior from the point of view of crystallite size values as a function of selenization temperature: crystallite size decreases slightly when selenization temperature increases from 200 °C to 300 °C, then it returns to increase, reaching the maximum values at 400 °C. Then, the crystallite size values decrease when temperature was raised to 500 °C. It seems that 400 °C is the temperature related to the maximum growth of crystallites, after that, the crystallites start to break, forming smaller grains on the surface. These facts can indicate that the growth of the crystallites is affected mainly by the selenization temperature, as well as by the phase formation, so indirectly by substrate nature. However, samples deposited onto silicon show different behavior, since the crystallite size value increases firstly when the temperature is raised to 300 °C, then it decreases slightly reaching the lower value (70.7 nm) at 500 °C. Indeed, films deposited onto glass at 300 °C, present the lower crystallite size. However, the highest crystallites were observed for the films deposited onto silicon at 300 °C. This occurrence suggests that besides the selenization temperature employed, substrate type plays an important role in crystal growth during the deposition of the films. It is evident from phase forming and Table 1 that the films deposited onto silicon substrates have a phase formation offset compared to the others films, besides reaching the highest grain size. This fact may be related to the physical properties of substrate that can speed up or slow down the phase formation.

Various microstructure parameters, such as dislocation density (δ) and microstrain (ε), were estimated from the XRD. To estimate the dislocation density, we have used the following expression from Williamson & Smallman (Thanikaikarasan et al., 2009), which allows obtaining the minimum dislocation density, used frequently for determining this parameter in semiconducting materials (Alkhayatt and Hussian, 2017; Kennedy et al., 2017; Bhuvaneswari et al., 2017; Derbali et al., 2018)

$$\delta = \frac{1}{D^2} \quad (2)$$

Being D the crystallite size.

To determine the microstrain, we have used the expression below (Klug and Alexander, 1974)

$$\varepsilon = \frac{\beta}{4tg\theta} \quad (3)$$

where β is the width at half-maximum (FWHM) and θ is the diffraction Bragg angle. The obtained values were summarized in Table 2. It can be seen that the dislocation density estimation obtained and the microstrain values are inversely proportional to the crystallite size values.

For both glass and alumina substrates, δ values increase when temperature raises from 200 to 300 °C, thereafter both ε and δ values decrease when the temperature raises up to 400 °C, then back to increase when temperature was raised to 500 °C. The microstrain of the deposited films reaches a

Table 1 Values of the crystallite size of SnSe films as a function of selenization temperatures and substrates type.

	$\langle D \rangle_{moy}$ (nm)			
Temperatures (°C)	200	300	400	500
Glass	59.5	58.6	85.1	70.8
Silicon	87.7	99.4	82.4	70.7
Alumina	70.9	63.7	75.6	63.6

minimum value at 400 °C; this may be due to the decrease of the number of defects onto the film at this temperature, suggesting a more homogenous layer. However, the increase in both values (dislocation density and microstrain) at higher temperature for the films deposited onto silicon substrates may be due to the creation of the voids into the film, caused by the detachment of some Se atoms, involving an increase in the number of defects. Indeed, this observation is widely related to the increase in the thermal stress at higher temperatures, causing an increase in dislocation and microstrain values. On the other hand, the films deposited onto alumina substrates show a more stable behavior in both microstructural values when changing the temperature. Therefore, the lower dislocation density and microstrain of the film deposited onto silicon at 300 °C suggest the higher crystallinity of this film.

The difference in crystal behavior observed for the different cases can be attributed to the fundamental role of the substrates and more specifically to the thermal properties of the substrates. Glass, silicon and alumina present different properties as the specific heat, the linear thermal expansion, the thermal conductivity (Substrate Material Properties; Galbraith, 2015; Jiu et al., 2013). Furthermore, the similar properties of glass and alumina can explain the similar behavior of the films deposited onto these substrate types.

Based on numerical simulations, Illés et al. have shown that the thermal properties of a variety of substrates have significant effects on the heat transfer coefficient (HTC) and thereafter, on the formation of a condensate layer (Illés et al., 2016).

3.2. Elemental analysis

As already mentioned in the characterization section, the Energy Dispersive X-ray Spectroscopy (EDAX) was used to determine the elemental composition of the obtained films. Table 3 summarized the atomic ratio of the SnSe thin films.

EDAX analysis has confirmed the presence of different atoms into the films and especially, the presence of oxygen into the films deposited onto glass and alumina at 500 °C. No phosphorus neither carbon was detected within the films, while the presence of other tin selenide phases as $SnSe_2$ were detected by a ratio $R_{Sn/Se} < 1$, which agree well with the XRD results. The EDAX pattern of the SnSe thin film deposited onto alumina showed the presence of Sn and Se peaks but the stronger peaks are related to substrate elements. For the films deposited onto silicon substrates at 400 °C, an atomic ratio of 0.92 was observed, yet the XRD results show the presence of both SnSe and $SnSe_2$ phases. This value very close to 1 suggest that the main phase formed onto this film is SnSe, while the amount of $SnSe_2$ should be very low (Fig. 4).

Nevertheless, the EDAX results is not consistent with the XRD analysis when the film was deposited onto alumina at 200 °C, since XRD analysis indicate that the obtained film was formed by a pure SnSe phase, however the EDAX analysis show that the atomic ratio of this film is higher than the stoichiometric value (Sn/Se = 1.26) as in the case of silicon substrate. Nevertheless, the peaks corresponding to metallic Sn in the XRD analysis probably have been masked by the high peaks corresponding to Al_2O_3 from the substrate. Similar observation was made for the film deposited onto alumina at 300 °C. This fact suggest that some peaks related to Sn phase are present onto these films, but masked by the Al_2O_3 peaks, which have very high intensities.

The obtained phases at different temperature and substrate type, according to the XRD results, confirmed by the EDAX analysis, are reported in Table 4.

3.3. Morphological properties

Using the scanning electron microscope (SEM) as a convenient technique, the surface morphology of the as-deposited films was studied at 5000 times magnification. The SEM pictures of SnSe thin films prepared at different selenization temperatures onto glass, silicon and alumina substrates are shown in Figs. 5a–5c respectively.

From the overall view of the SEM pictures, it can be derived that the films deposited at 200 °C and 300 °C onto glass and at 200, 300 and 400 °C onto silicon substrates are uniform and have very similar surface morphology. The surface is formed by spherically-shaped grains with a total coverage of the substrate. As the selenization temperature increased, the surface morphology of SnSe films deposited onto glass and silicon substrates becomes less homogeneous. Also, it is noticeable that when reaching 400 °C, the surface morphology of the samples deposited onto glass substrates becomes formed by big crystallites, involving a gradual increase in size, which is consistent with the calculated crystallite size values. Chandraa et al. (2007) reported similar observations about the increase in particle size when increasing the temperature for tin selenide thin films deposited by flash evaporation. However, the morphology of the films deposited at 400 °C onto silicon substrate is not in agreement with the crystallite size calculation, reaching at 500 °C a morphology similar to the one observed for the sample on glass at 400 °C.

When increasing the temperature up to 500 °C, the surface morphology of the films deposited onto glass substrates changed noticeably and the surface seems to be more flat and the forms of grains become not clearly identified. Apparently, grains break in smaller crystallites, allowing the formation of less dense and smooth films, with notable pores and voids. This observation is in agreement with XRD results, since the crystallite size values decrease at 500 °C and the microstructural parameters (ε and δ) increase.

Table 2 Micro structural properties of SnSe thin films.

	Temperatures (°C)	Dislocation density (δ) (10^{14} m^2)	Microstrain (ε) (10^{-3})
Glass	200	2.822	2.232
	300	2.911	1.993
	400	1.38	1.566
	500	1.994	2.100
Silicon	200	1.298	1.637
	300	1.010	1.393
	400	1.469	1.591
	500	1.999	1.845
Alumina	200	1.986	1.430
	300	2.459	1.608
	400	1.745	1.378
	500	2.465	1.467

All the films deposited onto alumina show similar morphology to those deposited onto other substrates at lower temperatures, but with a larger size of grains, which is in agreement with the evaluated crystallite size.

The pure SnSe morphology is in concordance with that observed by Sanjeeviraja et al. for SnSe films deposited by electrodeposition and annealed at 200 °C for 30 min (Subramanian et al., 1999). The dissimilar morphology observed for pure SnSe thin films deposited at 200 and 400 °C onto glass confirms that morphology is affected by the selenization temperature. Samples deposited at 500 °C onto glass and alumina substrates that consist of a mixture SnSe and SnO_2 phases, show a granular morphology, where the crystals are more clearly identified and easier observable. The difference in morphology for this type of mixed phase can be justified by the difference in microstructure properties and can be related, mainly, to the effect of substrate type, affecting the stoichiometry of the phases into the film. The obtained results show that morphology was widely affected by the obtained phase, selenization temperature and faintly by the type of substrate used.

Kumar et al. using thermal evaporation, have obtained a similar morphology to the one obtained by us under similar conditions, that is 500 °C temperature and glass substrate (Kumar et al., 2010). Indirajith et al. have studied the impact of the deposition temperature on the surface morphology of SnSe films deposited onto glass substrate by thermal evaporation in the range of 150–450 °C (Indirajith et al., 2010). Nevertheless, the obtained morphology is completely different to ours for all the temperature range, what can be associated to the different deposition method. However, authors declare that increasing the substrate temperature occurs appreciable changes in the surface morphology, as we have stated in our analysis

3.4. Film thickness

The film thickness of the films deposited onto glass and silicon substrates was determined using a cross-section observation. In Table 5 are summarized those results. In the case of alumina substrate, the presence of Pt electrodes on the substrate does not allow this measurement in a reliable way.

As shown in this table, regardless the substrate nature, the film thickness increase with increasing selenization temperature until reaching the maximum values at 400 °C. Above this temperature, the film thickness undergoes falling. The thickness values are higher for the films deposited onto silicon substrate except for the sample deposited at 400 °C. The extreme reduction in thickness when the temperature is raised to 500 °C for the sample deposited onto glass is in accordance with the results observed by SEM, suggesting that Se is detached from the layer, while the tin is oxidized, as observed by XRD and EDAX analysis.

3.5. Topographical properties

In order to visualize the surface topography of the as deposited films, study the growth evolution, and determine the impact of both selenization temperature and substrate type on the quality of the obtained films, AFM analysis was used. Figs. 6a–6c illustrates the AFM (2D view) topography of SnSe films deposited onto glass, silicon and alumina substrates respectively, at various selenization temperatures, scanned in a 5 μm × 5 μm area.

It is clear from the AFM images that the SnSe films covered all the glass substrate surface except at 500 °C where some flat areas appear. These flat areas were more observable when films were deposited onto silicon substrate, mainly at 300 and 400 °C. On the other hand, the AFM images of the films deposited onto alumina substrates show a complete coverage. It seems that the shape of the grains varied when changing selenization temperature and phase obtained. The best coverage was obtained for the films deposited onto alumina. The AFM images indicate that the selenization temperature, as well as the substrate nature, have a significant effect on the topology of the films.

The measured mean square root roughness (RMS) of the obtained films is shown in Table 6. The RMS values show that all samples have a low roughness, which varies between 0.48 and 0.89 nm. For the films deposited onto glass and silicon substrates, the RMS values follow the same behavior than the grain size with temperature: in both cases the values increase when increasing the temperature, reaching a maximum value at 400 °C and decreasing for 500 °C; This suggests that the increase in crystallite size affects the surface roughness of the layers. On the other hand, the films deposited onto alumina substrate are slightly rougher than other samples and the behavior of the RMS value does not match the behavior of the crystallite size. In this case, perhaps the initial roughness of the substrate (significantly higher than the roughness of the other type of substrates) affects these results.

3.6. Optical properties

As it is well known, transmittance and reflectance provide an estimation of the optical constants required for optoelectronic applications. Therefore, in order to study the effect of substrate and temperature on the optical properties of the as-deposited films, the optical transmittance (%T) and reflectance (%R) were measured and recorded in the wavelength range 250–2500 nm. Figs. 7a and 7b show the optical spectra of the films deposited at different selenization temperatures onto glass and silicon substrates, respectively.

Table 3 Atomic ratio $R_{Sn/Se}$ of different SnSe thin films deposited.

Substrates	Glass				Silicon				Alumina			
Temperatures (°C)	200	300	400	500	200	300	400	500	200	300	400	500
$R_{Sn/Se}$	1.19	0.76	1.01	1.31	1.24	0.74	0.92	1.12	1.26	0.7	1.04	2.23

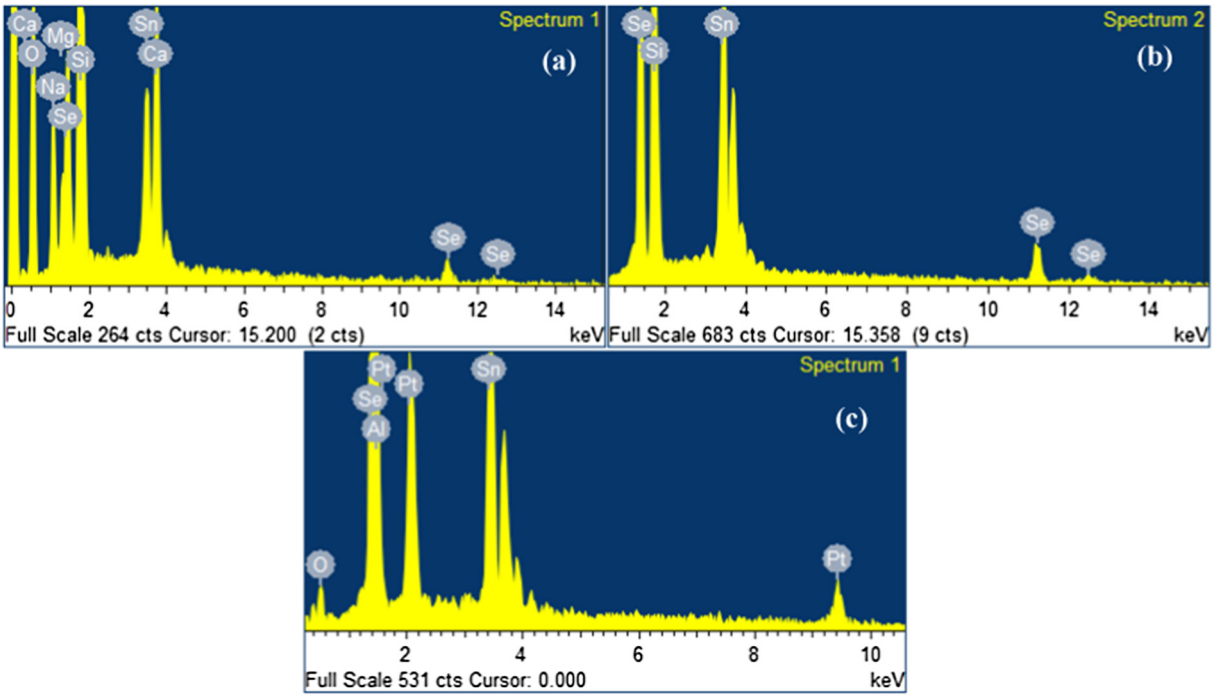

Fig. 4 EDAX patterns of SnSe films deposited onto glass (a), silicon (b) and alumina (c) substrates at 200 °C.

Table 4 The obtained phases as a function of selenization temperatures and substrates type.

Substrat	Temperature (°C)			
	200	300	400	500
Glass	SnSe	SnSe + $SnSe_2$	SnSe	SnSe + SnO_2
Silicon	Sn + SnSe	SnSe + $SnSe_2$	SnSe + $SnSe_2$	SnSe
Alumina	SnSe	$SnSe_2$	SnSe	SnSe + SnO_2

Analyzing the transmittance curves of the films deposited onto silicon substrates, samples present a constant low transmittance in the wavelength region lower than 1000 nm, which is expected due to the low transparency of the silicon wafer. Nevertheless, the sample deposited at 500 °C, formed by pure SnSe phase, shows the highest transmittance ≈ 12% in this region, even for wavelengths above this region, reaching values over 40%. The transmittance to wavelength behavior for all the samples is very similar, but reaching different values. As mentioned, the layer deposited at 500 °C show the highest transmittance, followed by the sample deposited at 300 °C, the one deposited at 400 °C and, finally the lowest values are associated to the sample deposited at 200 °C, that presented metal tin mixed with SnSe.

The high transmittance observed for the samples deposited onto glass compared to those deposited onto silicon may be related to the high transmittance of the glass itself, mostly in the lower wavelength range. The highest values in all the spectra correspond to the layer deposited at 400 °C, which is formed by SnSe, with no other phases. In this case, the values are higher than 50% for wavelengths over 1250 nm in the IR region. There is another peak at the UV region around 45%. In the visible region, the transmittance value is near 35%. The layer deposited at 500 °C, which presented traces of tin oxide, follows the same behavior, but with lower values, reaching a transmittance value near 40% for the higher wavelengths. The lowest values correspond to the layer deposited at 200 °C, reaching a maximum near 30%. Finally, the layer deposited at

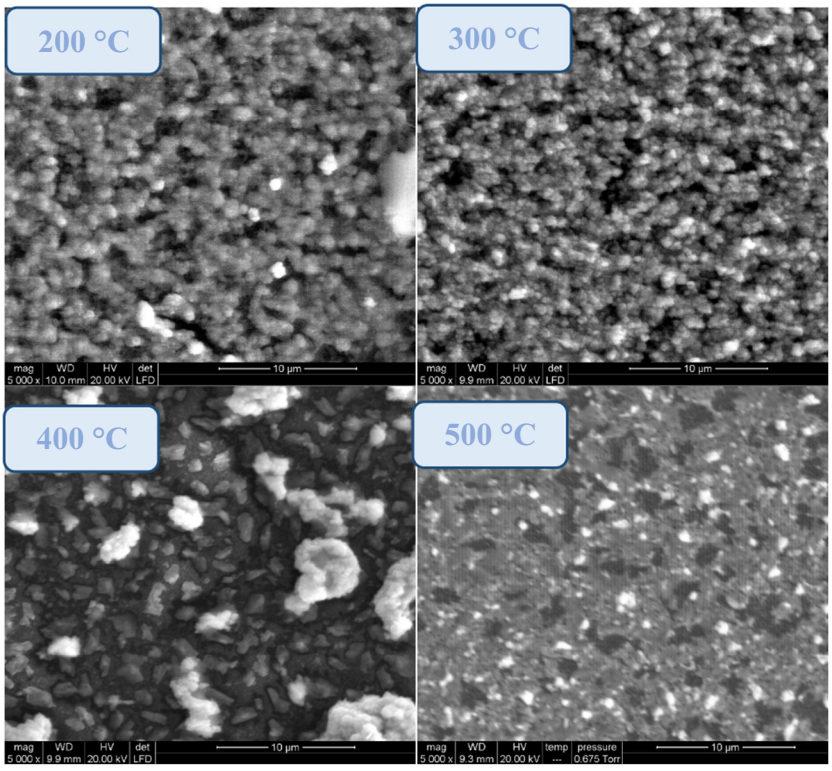

Fig. 5a SEM pattern of SnSe films prepared onto Glass substrate at various selenization temperatures.

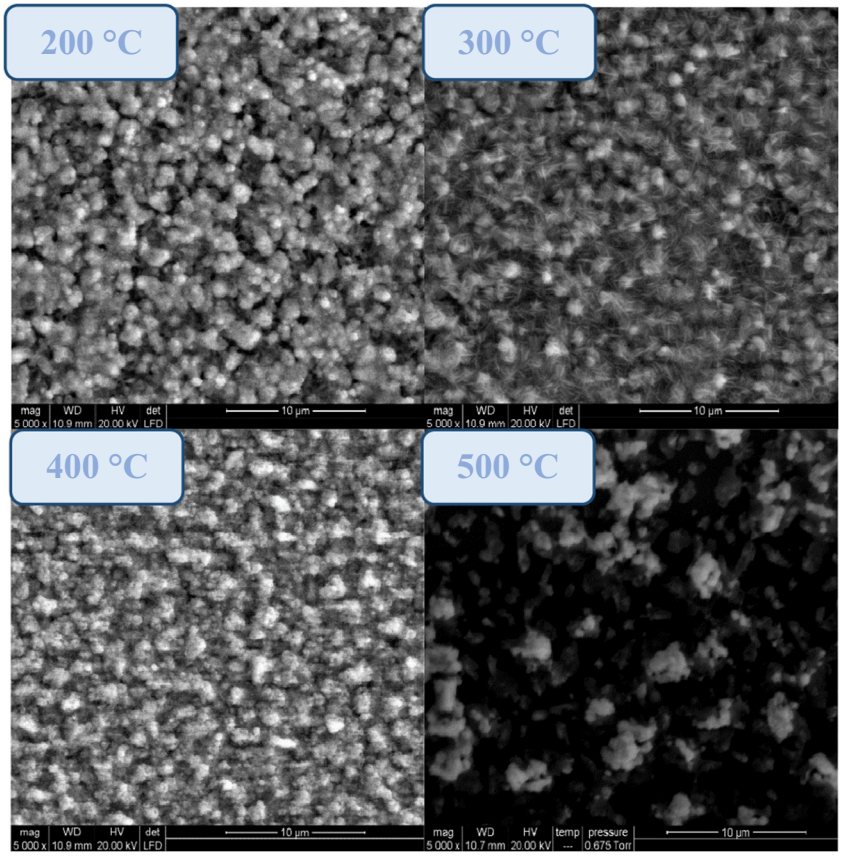

Fig. 5b SEM pattern of SnSe films prepared onto Silicon substrate at various selenization temperatures.

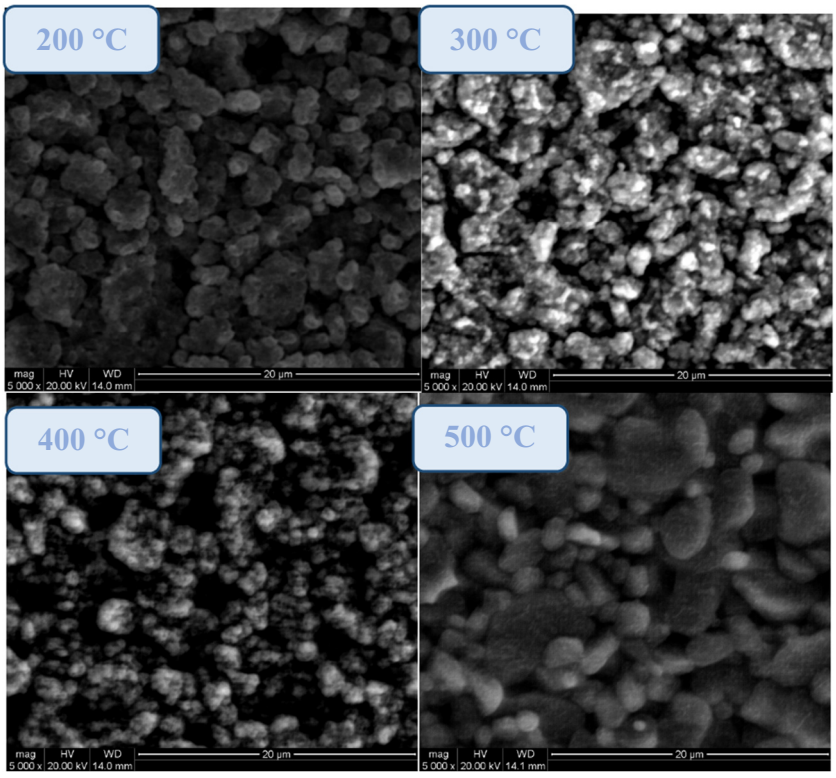

Fig. 5c SEM pattern of SnSe films prepared onto Alumina substrate at various selenization temperatures.

300 °C shows a slightly different behavior, since for wavelengths lower than 1250 nm this layer shows a continuous increase in the transmittance values, not observed for the other layers tested. For wavelength values higher than 1250 nm, the transmittance shows also a continuous increase, but with a lower slope, reaching the same maximum value than the layer with best overall performance at the highest wavelengths.

The increase in transmittance values in the higher wavelength range for different samples can be a good indicator of the homogenous nature of the as-obtained films.

An overview to the optical reflectance spectra of the samples show that all the films exhibit a similar behavior, with a slight change in reflectance as a function of temperature. Samples deposited onto silicon have a higher optical reflectance at very low wavelength range, decreasing to a reflectance values lower than 20% for wavelengths over 500 nm. Contrariwise, for those samples deposited onto glass substrates the maximum of transmittance does not exceed 40% in the UV region. The high reflectance observed for the films deposited onto silicon is related to the nature of the substrate itself.

Based on the obtained results, the effect of substrate type on the transmittance and the reflectance behavior is very consistent. The results seem to indicate that the pure SnSe layers show the highest values of transmittance.

In order to study more deeply the effect of these factors on the optical properties of the as-deposited films, absorption spectra between 250 and 2500 nm were evaluated using the optical transmittance and reflectance data, through Eq. (4), where T and R are the transmittance and reflectance, respectively and d is the film thickness (Barreau et al., 2001).

$$\alpha = \frac{1}{d} Ln \frac{(1-R)^2}{T} \tag{4}$$

Fig. 8 shows the spectral dependence of absorption coefficient α as a function of photon energy for different samples in the range of 250–2500 nm.

As shown from the plot (Fig. 8), all samples possess an optical absorption in the order of 10^4 cm^{-1} in the UV–visible-NIR region, indicating that the obtained films were highly absorbing, being suitable for photovoltaic applications. It is also clearly observed that the samples have a large absorption region that extends to the IR region. Remarkably, the presence of oxygen into the films deposited onto glass substrate or the metallic tin into the films deposited onto silicon

Table 5 The obtained film thickness of the samples deposited onto glass and silicon substrate at different selenization temperatures.

Substrat	Thickness (nm)			
	200 °C	300 °C	400 °C	500 °C
Glass	457	549	935.5	263.2
Silicon	564	685.5	854.5	712

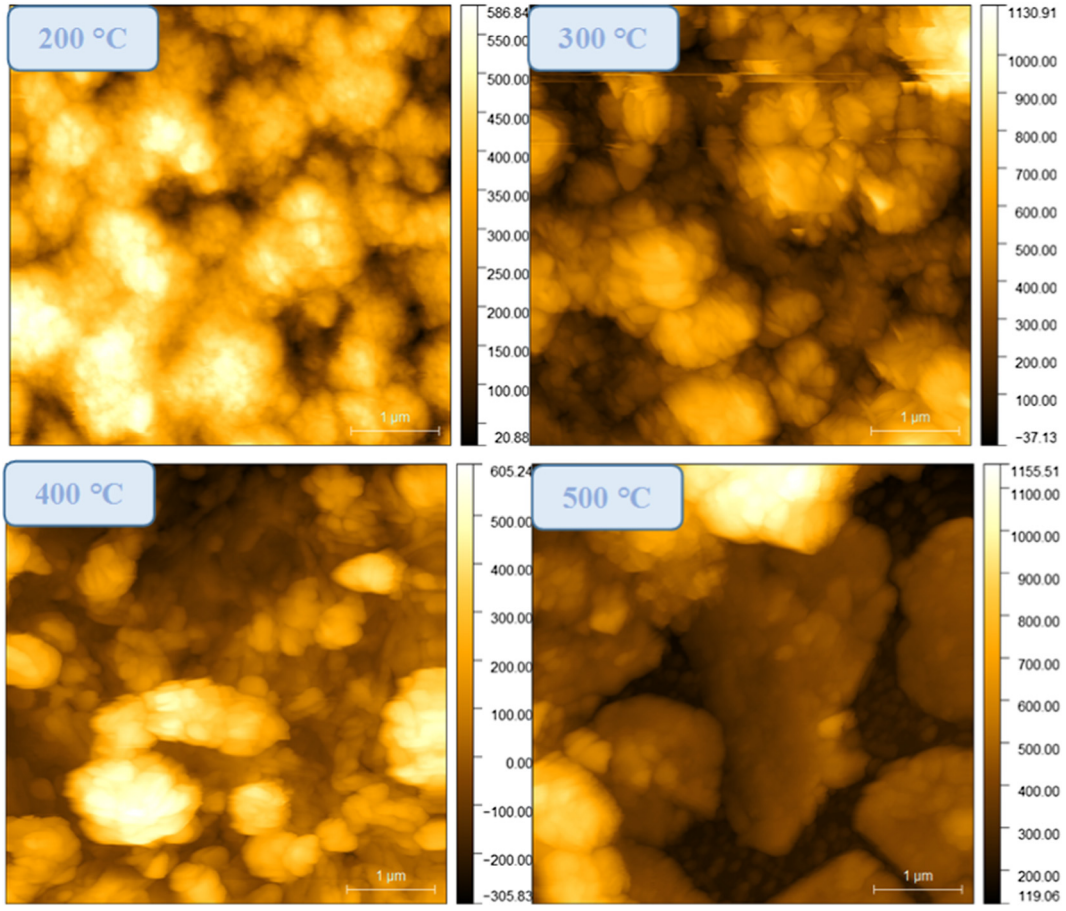

Fig. 6a AFM images of the SnSe films deposited onto glass substrates at various selenization temperatures.

substrates allows increasing the optical absorption coefficient. However, the films containing only SnSe phase possess the lower α values. Subsequently, the presence of mixed phases within the films allows an enhancement in the optical absorption coefficient.

In order to estimate the band gap of the as deposited materials and to identify the type of transition, $(\alpha h\upsilon)^n$ versus $h\upsilon$ were plotted based on Tauc and Abeles theory (Tauc and Menth 1972) given by the following expression (5)

$$(\alpha h\upsilon)^n = A(h\upsilon - E_g) \quad (5)$$

where A is a constant, α is the absorption coefficient, $h\upsilon$ is the photon energy, n is an index related to the type of transition (n = ø for indirect allowed transition, n = 2 for direct allowed transition, n = 1/3 for indirect forbidden transition and n = 2/3 for direct forbidden transitions). Based on that plot, the optical band gaps are obtained by the intercept of the straight-line portion with the photon energy axis. The best-obtained straight line was observed when n = 2 for all the samples, which assigns the direct allowed transitions to the obtained films.

Fig. 9 shows the Tauc plot of the different obtained films and their relative optical band gap. It was clearly shown from the obtained values that the optical band gap of the tin selenide films were affected by the selenization temperature. It was found that the band gap energy values of the pure tin selenide films deposited onto glass substrate was equal to 0.95 eV, independently to the selenization temperature (200 or 400 °C). However, the change of energy band gap observed for other samples can be related to the formation of mixed phases, as supported by the X-ray diffraction results, reported above. The presence of $SnSe_2$ over to SnSe for film deposited onto glass at 300 °C leads to a displacement in band gap values towards higher values. This is not surprising since $SnSe_2$ have an optical band gap (1.48 eV), higher than SnSe.

Meanwhile, it is well known that optical properties could be influenced by many other parameters such as thickness, grain size, defects, structural parameters, presence of vacancies, surface roughness, etc. Moreover, a decrease in gap energy values was observed for the films deposited onto glass substrates when selenization temperature reached 500 °C. This unexpected fact cannot be related only to the presence of tin oxide phase, because the band gap of SnO_2 is higher than SnSe and $SnSe_2$ band gap, contrariwise it can be assigned to the high dislocation density values and lattice strain revealed by structural studies.

The E_g values of tin selenide films obtained in the present work matched very well with those reported earlier for SnSe thin films deposited by other techniques (Subramanian et al., 1999; Indirajith et al., 2010; Mariappan et al., 2010) that confirm it as a promising candidate for solar cells application (see Table 7).

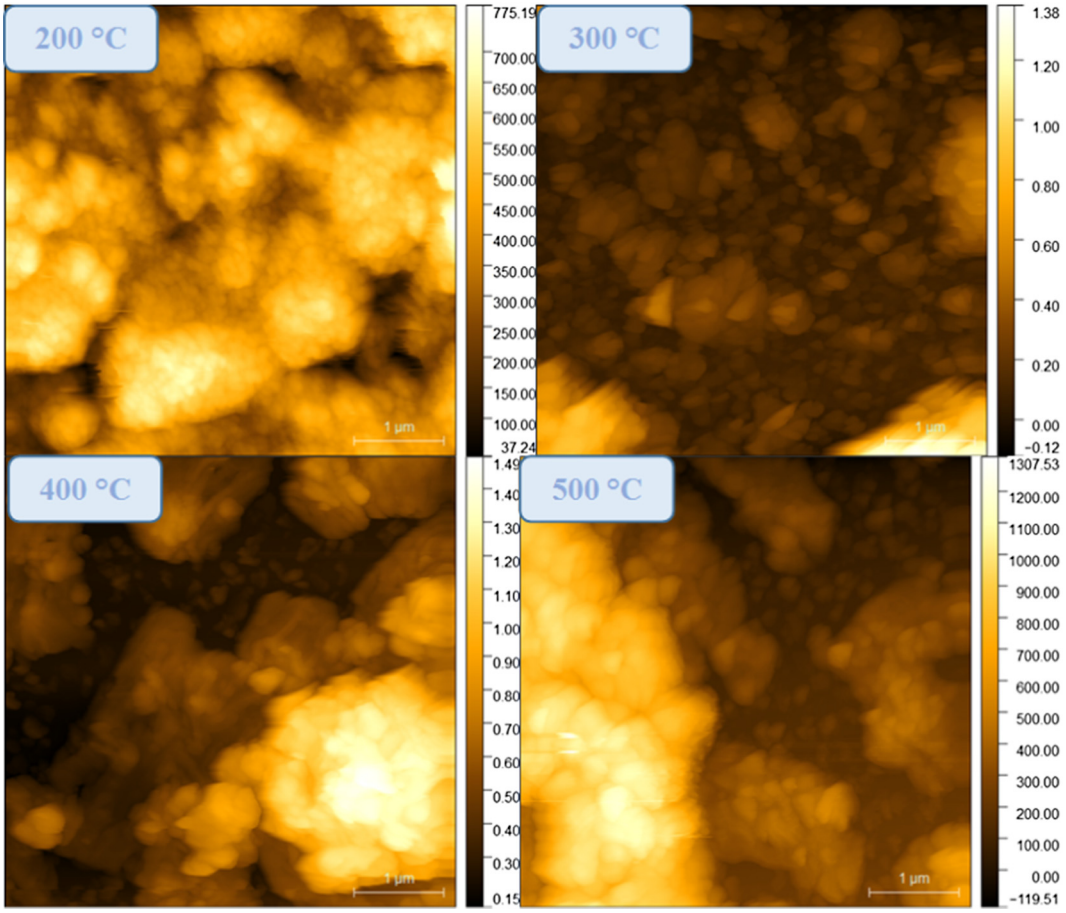

Fig. 6b AFM images of the SnSe films deposited onto silicon substrates at various selenization temperatures.

3.7. Gas sensing properties

In addition to the structural and morphological properties, sensing properties of SnSe thin films deposited onto alumina substrate were investigated for the first time. Gas sensing studies of our sensors were performed monitoring the sensor resistance changes due to the interaction between the gas molecules and the sensor material surface.

The initial characterization was carried out under methane gas diluted in dry air with concentrations of 0.2%, 0.5% and 1%, respectively and setting an operating temperature for the sensors of 150 °C, below the deposition temperature of any sample. Under these conditions, the sensors deposited at 200 and 500 °C did not show any response. However, the samples deposited at 300 °C (mainly $SnSe_2$) and 400 °C (mainly SnSe) showed a weak response.

It is well known that the working temperature is a vital parameter, that influences widely the desorption and adsorption processes. For this reason, the operating temperature was raised up to 200 °C in order to improve the obtained results. As a result of this increase in the operating temperature, the sensor response of samples deposited at 300 and 400 °C were substantially improved from the point of view of sensitivity, stability and response/recovery times, while sensors deposited at 200 and 500 °C did not show any response. This fact indicates that an operating temperature of 200 °C can supply sufficient thermal energy, allowing the methane molecules to react with the sensor surface.

The response of sensors deposited at 400 °C (mainly SnSe) and 300 °C (mainly $SnSe_2$) when operated at 200 °C in presence of different concentration of methane are shown in Figs. 10 and 11 respectively. The sensors were exposed to the gas during 900 s, and to air during 1800 s.

After exposing the sensors to CH_4, the resistances of the samples decreased, confirming an *n*-type behavior of both SnSe and $SnSe_2$. When methane flow was stopped and the sensors were exposed just to dry air, the sensors resistance raised slowly and recovered the baseline, confirming the reversible interaction between the obtained sensing materials and methane gas.

Fig. 12 shows the plot of sensors response R variation as a function of methane gas concentration.

Obviously, for both sensors the reduction of resistance is proportional to methane concentration. SnSe sensor shows higher response than $SnSe_2$. This fact can be ascribed to the high surface porosity of the SnSe sensor in comparison to the $SnSe_2$ sensor.

Response and recovery times were evaluated for both sensors and depicted in Fig. 13 as a function of methane concentration.

It is clear that the response time decreases with increasing gas concentration, while the recovery time increases. It is also clear that SnSe sensor exhibited faster response and recovery

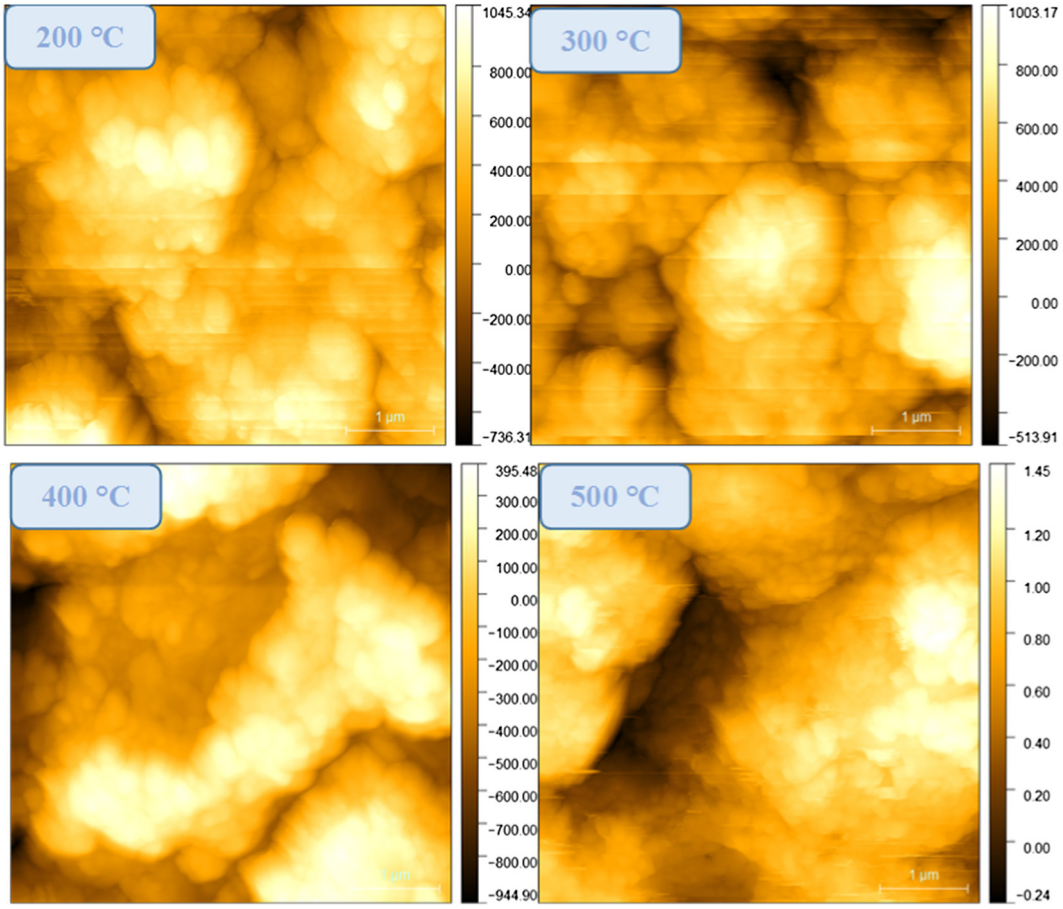

Fig. 6c AFM images of the SnSe films deposited onto alumina substrates at various selenization temperatures.

Table 6 RMS values of SnSe thin films.

Substrates	Glass				Silicon				Alumina			
Temperatures (°C)	200	300	400	500	200	300	400	500	200	300	400	500
RMS (nm)	0.48	0.69	0.73	0.48	0.49	0.63	0.66	0.58	0.89	0.7	0.59	0.77

Table 7 Band gap (Eg) values of SnSe thin films.

	Techniques	Substrates	Temperature (°C)	Eg (eV)	D (nm)
Present work	CVD	Glass	200	0.95	59.52
			300	1.35	58.60
			400	0.95	85.10
			500	0.93	70.81
65	Spray pyrolysis	Non-conducting glass	350	1.08	≈48
35	Electrodeposition	TO-coated glass	55	1.05	≈5000
36	Thermal evaporation	Glass	150–450	0.6–1.2	8.35–63.02

time, regardless the gas concentration, which can be attributed to the high quality and the proper pore structure of SnSe sensor. Regarding the sensing mechanism, it is not clear and should be investigated. In the case of SnS/SnS_2, similar compounds, two different mechanisms have been suggested, and can be also considered for $SnSe/SnSe_2$. Ou et al. (2015) have proposed a physisorption with charge transfer. On the other hand, Giberti et al. (2016) have suggested that the surface of the SnS layer is oxidized and this absorbed oxygen, when reacting with the surrounding gases, is the base of the trans-

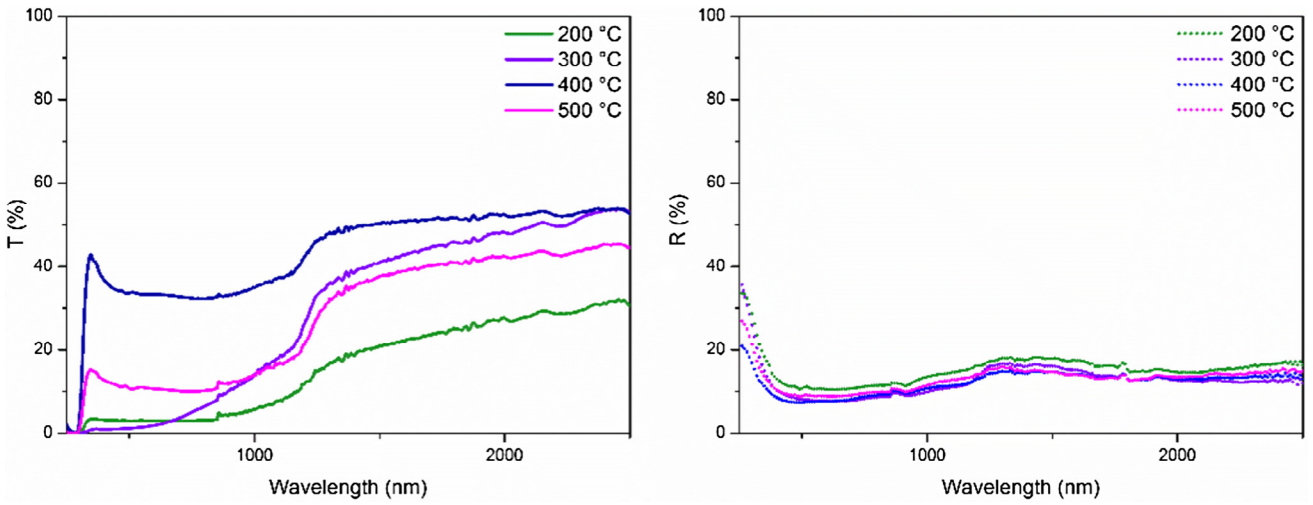

Fig. 7a Optical Transmission and Reflectance spectra of SnSe films deposited onto Glass substrate at various selenization temperatures.

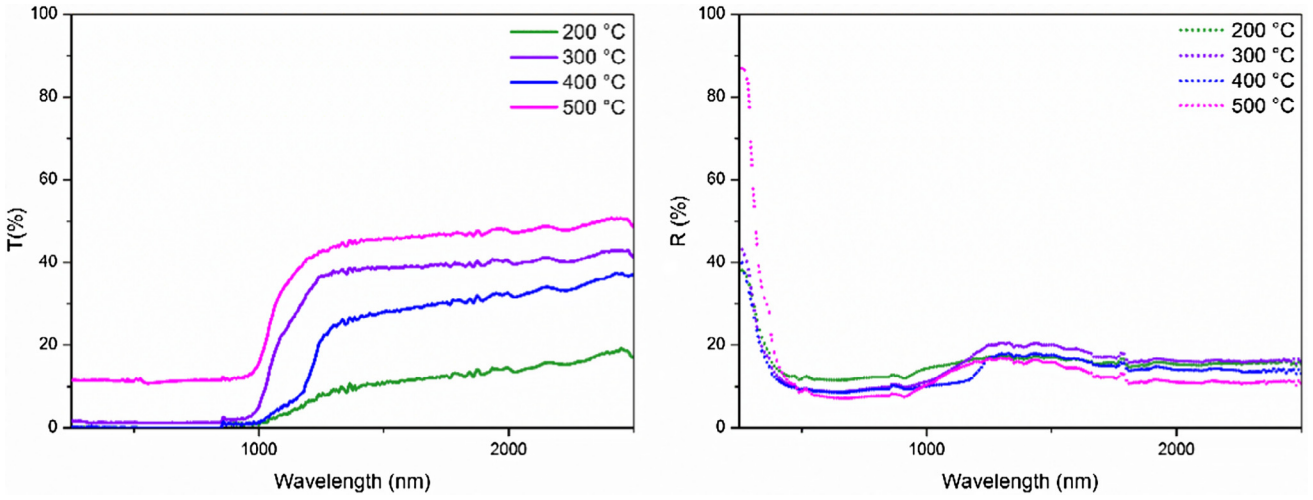

Fig. 7b Optical Transmission and Reflectance spectra of SnSe films deposited onto Silicon substrate at various selenization temperatures.

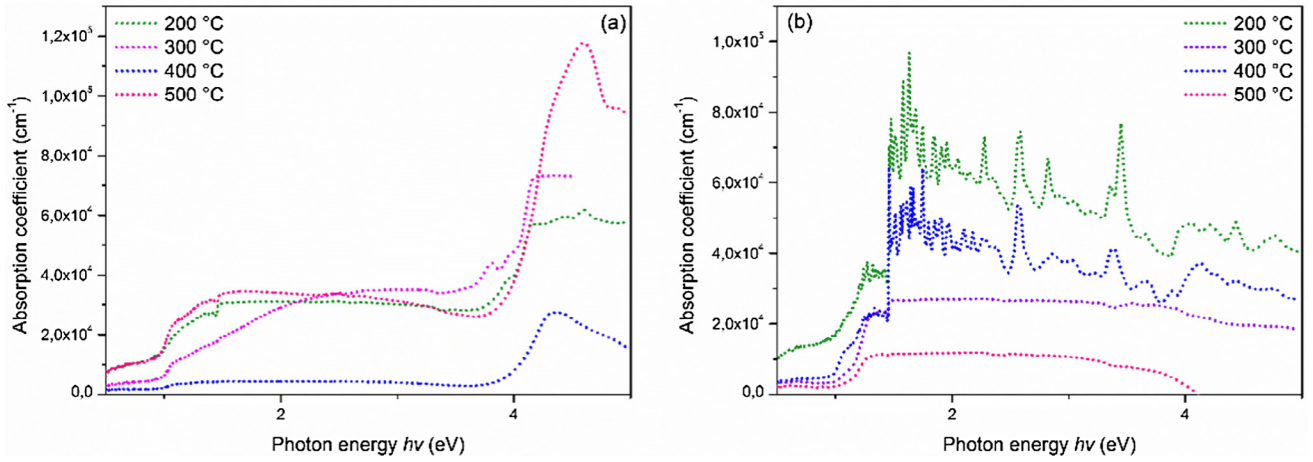

Fig. 8 Optical absorption coefficient versus photon energy for SnSe films deposited onto glass (a) and silicon (b) substrates at various selenization temperatures.

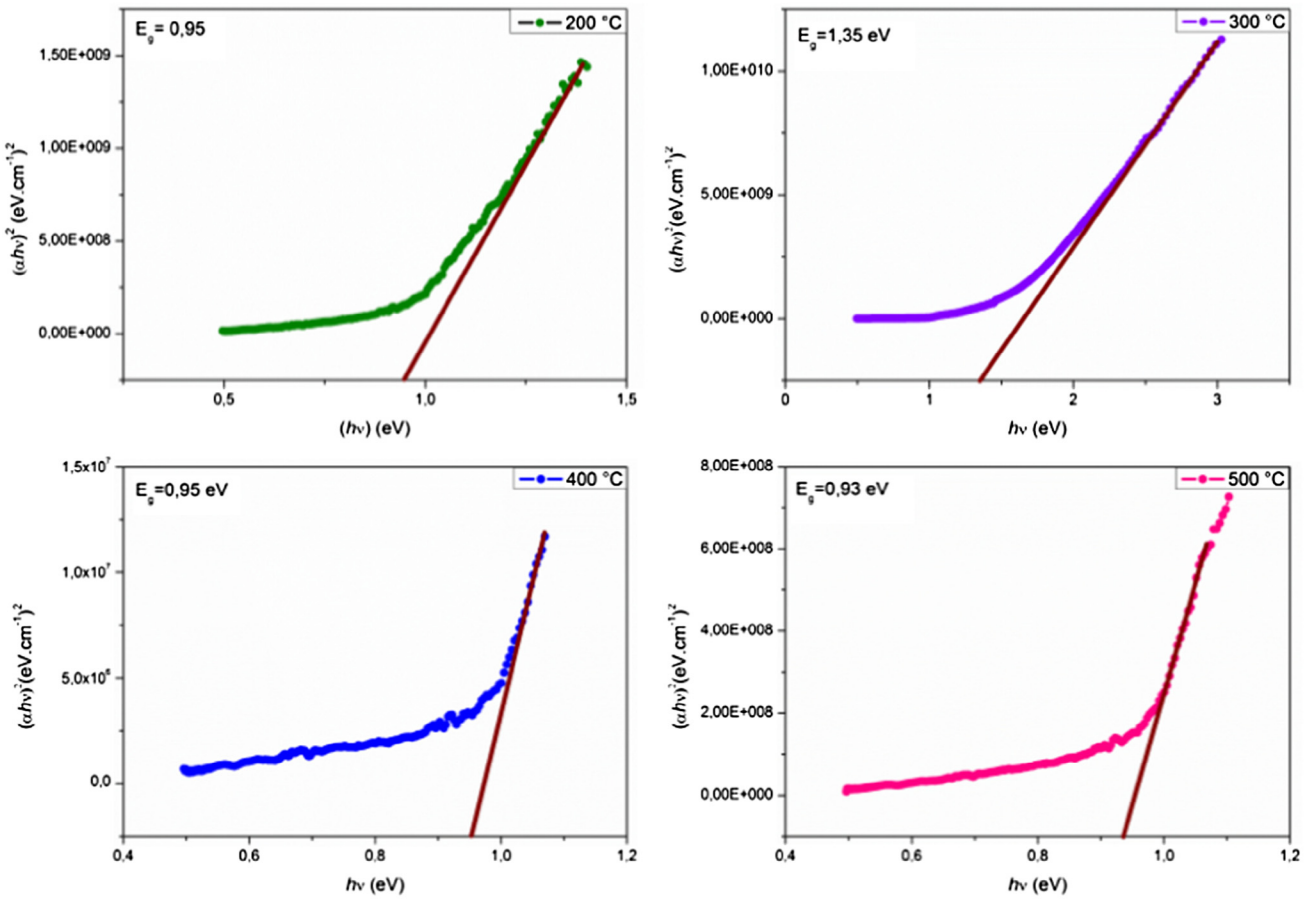

Fig. 9 Tauc plot $(\alpha h\upsilon)^2$ versus photon energy ($h\upsilon$) for SnSe films deposited onto glass substrate at 200 °C, 300 °C, 400 °C and 500 °C.

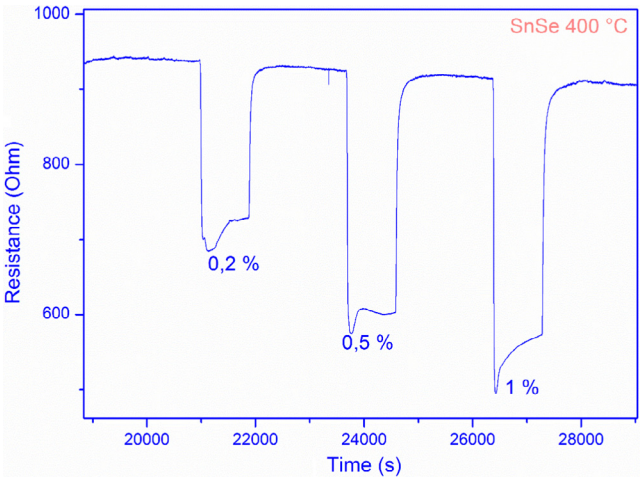

Fig. 10 Response of SnSe sensor (deposited at 400 °C) to different methane concentration at operating temperature of 200 °C.

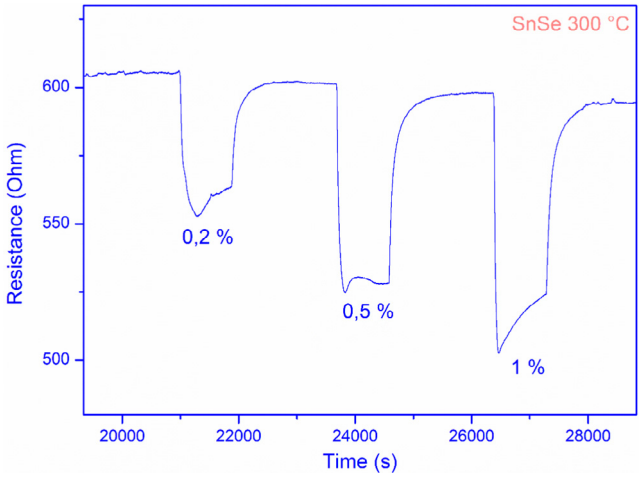

Fig. 11 Response of $SnSe_2$ sensor (deposited at 300 °C) to different methane concentration at operating temperature of 200 °C.

duction process. This second mechanism is supported by Kergommeaux et al. (2012), that have proved the Sn oxidation state using ^{119}Sn-Mössbauer spectroscopy in SnS layers, deposited by different methods, after some minutes exposed to air. The response behavior of SnSe and $SnSe_2$ sensors towards various other gases is under investigation.

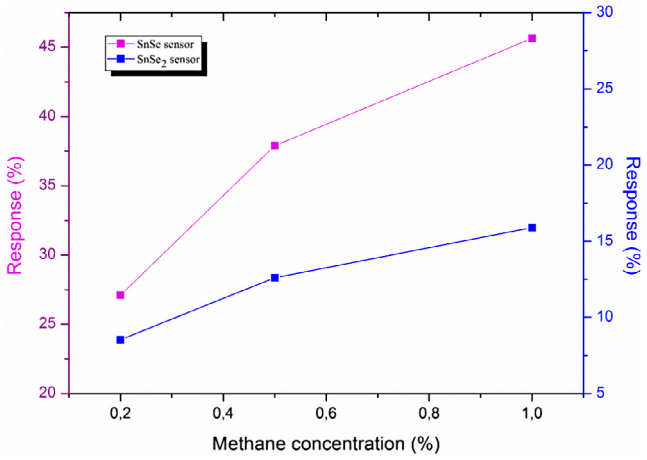

Fig. 12 Plot of the sensors response operated at 200 °C as a function of methane concentration.

4. Conclusion

In summary, a novel organophosphorus compound was used as a selenium precursor to prepare SnSe films by means of the CVD technique in a temperature range from 200 to 500 °C. Structural, morphological, optical and electrical properties of the obtained SnSe thin films were investigated. It was found that the influence of substrate type and selenization temperature on different properties of as-obtained film was significant. XRD analysis confirmed the formation of a SnSe phase at lower temperature. Then, with increasing selenidisation temperatures, mixed phases as $SnSe_2$ appears along with SnSe and at higher temperature a remarkable appearance of SnO_2 phase was observed. Substrate type plays a key role in the rate of appearance of each phase. XRD diffraction pattern confirms orthorhombic structure with (1 1 1) preferred orientation of all SnSe obtained and the estimated grain size shows its highest values at 400 °C. Additionally, the structural, micro structural, optical and electrical properties of the obtained films were greatly influenced by the substrate type and selenization temperature and, hence, by the phase obtained. It was seen that the incorporation of $SnSe_2$ and SnO_2 into the films affected remarkably the properties of the deposited films. It was found that the optical properties correlated well with the microstructure results.

All obtained films exhibit a direct allowed transition with a band gap that varies between 0.95 and 1.35 eV. The high optical absorbance in a wide light region together with a low transmittance, assure the suitability of the obtained films for photovoltaic applications. The optical study suggests the usefulness of the obtained samples in photovoltaic structures because of the higher optical absorption coefficient. The obtained SnSe and $SnSe_2$ materials deposited onto alumina substrates show interesting sensing properties towards methane gas. SnSe sensor show a better sensitivity than $SnSe_2$ sensor at operating temperature of 200 °C. The obtained results suggest that SnSe can be a new promising material for chemoresistive gas sensing.

Acknowledgements

K. Assili and K. Alouani are grateful to Pr. E. Llobet for thoughtful and useful comments as well as for accepting the internship in his Research Group at the Department of Electronic, Electrical and Automatic Engineering of University Rovira i Virgili in Tarragona, Spain. K. Assili is thankful to Dr Raùl Calavia and Juan Casanova chafer for general assistance in the laboratory. Tunisian Ministry of Higher Education and Scientific Research (MHESR) is acknowledged for financial support through 'the Alternance Bourse' grant. This work has been funded in part by MINECO under grant no. TEC2015-71663-R.

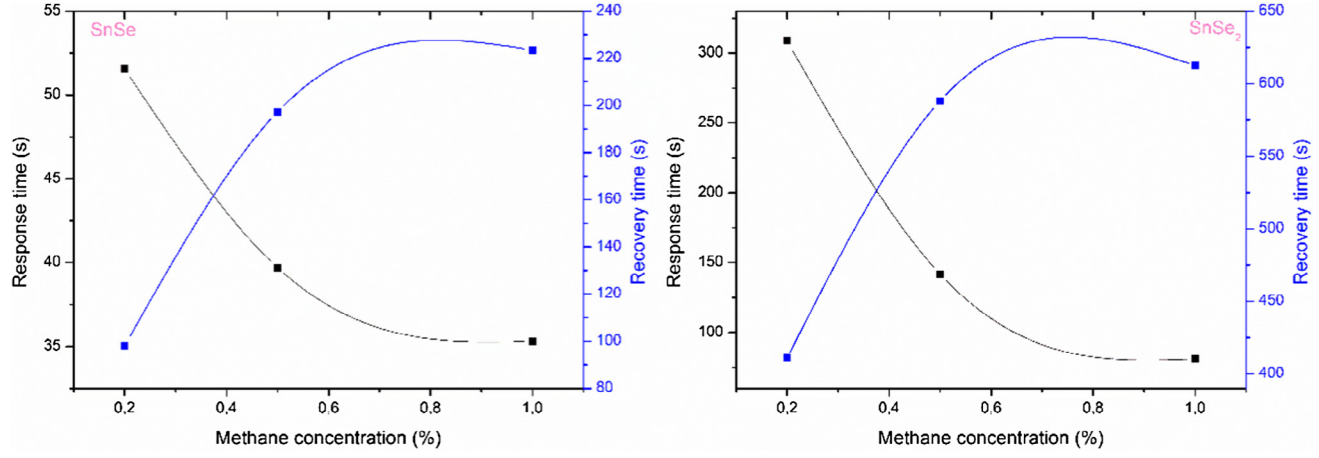

Fig. 13 Response and recovery time characteristics of SnSe and $SnSe_2$ sensors operated at 200 °C.

References

Opoku, F., Asare-Donkor, N.K., Adimado, A.A., 2015. Comput. Theor. Chem. 1058, 1–11.

Panneerselvam, A., Periyasamy, G., Ramasamy, K., Afzaal, M., Malik, M.A., O'Brien, P., Burton, N.A., Waters, J., Dongen, B.E. V., 2010. Dalton Trans. 39, 6080–6091.

Assili, K., Alouani, K., Vilanova, X., 2017. Semicond. Sci. Technol. 32, 1–11.

Afzaal, M., Crouch, D., O'Brien, Paul, 2005. Mater. Sci. Eng., B 116, 391.

Park, H., Afzaal, M., Helliwell, M., Malik, M.A., O'Brien, P., Raftery, J., 2003. Chem. Mater. 15, 4205.

Waters, J., Crouch, D., O'Brien, P., Park, JIN-Ho, 2003. J. Mater. Sci. Mater. Elec. 14, 599–602.

Afzaal, M., Aucott, S.M., Crouch, D., O'Brien, P., Woollins, J.D., Park, J.-H., 2002. Chem. Vap. Deposition 8, 187.

Panneerselvam, A., Malik, M.A., Afzaal, Mohammad, O'Brien, P., Helliwell, M., 2008. J. Am. Chem. Soc. 130, 2420–2421.

Garje, S.S., Copsey, M.C., Afzaal, M., O'Brien, P., Chivers, T., 2006. J. Mater. Chem. 16, 4542–4547.

Briand, G.G., Chivers, T., Parvez, M., 2002. Angew. Chem., Int. Ed. 41, 3468.

Chivers, T., Eisler, D.J., Ritch, J.S., 2005. Dalton Trans., 2675

Kim, S., Duong, A., Cho, S., Rhim, S.H., Kim, J., 2016. Surf. Sci. 651, 5–9.

Guan, X.H., Lu, P.F., Wu, L.Y., Han, L.H., Liu, G., Song, Y.X., Wang, S.M., 2015. J. Alloy Compd. 643, 116–120.

Singh, N.K., Bathula, S., Gahtori, B., Tyagi, K., Haranath, D., Dhar, A., 2016. J. Alloy Compd. 668, 152–158.

Baumgardner, W.J., Choi, J.J., Lim, Y.-F., Hanrath, T., 2010. J. Am. Chem. Soc. 132, 9519.

Pejova, B., Tanuševski, A., 2008. J. Phys. Chem. C 112, 3525.

He, X., Shen, H., Wang, W., Wang, Z., Zhang, B., Li, X., 2013. J. Alloy Compd. 556, 86–93.

Shi, G., Kioupakis, E., 2015. Nano Lett. 15, 6926–6931.

Shi, G., Kioupakis, E., 2015. J. Appl. Phys. 117, 065103.

Anwar, S., Gowthamaraju, S., Mishra, B.K., Singh, S.K., Anwar, S., 2015. Mater. Chem. Phys. 153, 236–242.

Ferreiro, J.O.M., Diaz-Droguett, D.E., Celentano, D., Reparaz, J.S., Torres, C.M.S., Ganguli, S., Luo, T., 2017. Appl. Therm. Eng. 111, 1426–1432.

Anwar, S., Mishra, B.K., Anwar, S., 2016. Mater. Chem. Phys. 175, 118–124.

Heremans, J.P., 2014. Nature 508, 327–328.

Zhang, H., Talapin, D.V., 2014. Angew. Chem. Int. Ed. 53, 9126–9127.

Xu, X., Song, Q., Wang, H., Li, P., Zhang, K., Wang, Y., Yuan, K., Yang, Z., Ye, Y., Dai, L., 2017. ACS Appl. Mater. Interf. 9, 12601–12607.

Timofeev, Yu.A., Vinogradov, B.V., Begoulev, V.B., 1997. Phys. Solid State 39, 207.

Zhao, L., Tan, G., Hao, S., He, J., Pei, Y., Chi, H., Wang, H., Gong, S., Xu, H., Dravid, V.P., Uher, C., Snyder, G.J., Wolverton, C., Kanatzidis, M.G., 2016. Science 351, 141–144.

Kumar, V., Kumar, P., Yadav, S., Kumar, V., Bansal, M.K., Dwivedi, D.K., 2015. J. Mater. Sci.: Mater. Electron., 1–7

Ning, J., Xiao, G., Jiang, T., Wang, L., Dai, Q., Zou, B., Liu, B., Wei, Y., Chen, G., Zou, G., 2011. Cryst. Eng. Comm. 13, 4161–4166.

Zainala, Z., Nagalingama, S., Kassima, A., Husseina, M.Z., Yunusb, W.M.M., 2004. Sol. Energ. Mater. Sol. Cells 81, 261–268.

Mathews, N.R., 2012. Sol. Energ. 86, 1010–1016.

Popescu, M., Sava, F., Lorinczi, A., Socol, G., Mihailescu, I.N., Tomescu, A., Simion, C., 2007. J. Non-Cryst. Solids 353, 1865–1869.

Xue, M.Z., Yao, J., Cheng, S.C., Fu, Z.W., 2006. J. Electrochem. Soc. 153, A270.

Chung, K.M., Wamwangi, D., Woda, M., Wutting, M., Bensch, W., 2008. J. Appl. Phys. 103, 083523.

Subramanian, B., Mahalingam, T., Sanjeeviraja, C., Jayachandran, M., Juliana Chockalingam, M., 1999. Thin Solid Films 357, 119–124.

Indirajith, R., Srinivasan, T.P., Ramamurthi, K., Gopalakrishnan, R., 2010. Curr. Appl. Phys. 10, 1402–1406.

Zainal, Z., Saravanana, N., Anuara, K., Husseina, M.Z., Yunus, W. M.M., 2004. Mater. Sci. Eng. B 107, 181–185.

Butt, F.K., Mirza, M., Cao, C., Idrees, F., Tahir, M., Safdar, M., Ali, Z., Tanveera, M., Aslama, I., 2014. Cryst. Eng. Comm. 16, 3470–3473.

Wang, J., Lv, A., Wang, Y., Cui, B., Yan, H., Hu, J., Hu, W., Guo, Y., Wan, L., 2013. Sci. Rep. 3 (2613), 1–6.

Lou, Z., Li, F., Deng, J.N., Wang, L.L., Zhang, T., 2013. ACS Appl. Mater. Interf. 5, 12310–12316.

Boudjouk, P., Seidler, D., Grier, D., McCarthy, G., 1996. Chem. Mater. 8, 1189.

Biçer, M., Sisman, I., 2011. App. Surf. Sci. 257, 2944–2949.

Busch, G., Froehlich, C., Hulliger, F., Helv, F., 1961. Phys. Acta 34, 359.

McCarthy, G., Welton, J., 1989. Powder Diffr. 4, 156.

Fernandes, P.A., Sousa, M.G., Salomé, P.M.P., Leitão, J.P., da Cunha, A.F., 2013. Cryst. Eng. Comm. 15, 10278.

Tatge, S., 1953. Natl. Bur. Stand. (U.S.), Circ. 539, I, 24.

Colin, R., Drowart, J., 1964. Trans. Faraday Soc. 60, 673.

Wieihcmei, H., Pultz, G., 1983. Z. anorg. allg. Chem. 499, 130–144.

Sharma, R.C., Chang, Y.A., 1986. Bull. Alloy Phase Diagr. 7, 68.

Scherrer, P., Von Der Gesellschaft Der Wissenschaften Zu Göttingen, N., 1918. Math. Klasse. 98–100.

Thanikaikarasan, S., Mahalingam, T., Sundaram, K., Kathalingam, A., Kim, Y.D., Kim, T., 2009. Vacuum 83, 1066–1072.

Alkhayatt, A.H.O., Hussian, S.K., 2017. Surf. Interf. 8, 176–181.

Kennedy, A., Kumar, V.S., Raj, K.P., 2017. J. Phys. Chem. Solids 110, 100–107.

Bhuvaneswari, P.V., Ramamurthi, K., Babu, R.R., 2017. Thin Solid Films 632, 44–49.

Derbali, A., Attaf, A., Saidi, H., Benamra, H., Nouadji, M., Aida, M. S., Attaf, N., Ezzaouia, H., 2018. Optik 154, 286–293.

Klug, H.P., Alexander, L.E., 1974. Wiley, New York.

Substrate Material Properties, <http://www.yourthinfilm-source.com/substrate-material-properties/>.

Galbraith, J., 2015. Glass Thermal Properties and Their Role in Product Design, <http://www.koppglass.com/blog/glass-thermal-properties-and-their-role-in-product-design/>.

Jiu, J., Sugahara, T., Nogi, M., Araki, T., Suganuma, K., Uchida, H., Shinozaki, K., 2013. Nanoscale 5, 11820–11828.

Illés, B., Géczy, A., Skwarek, A., Busek, D., 2016. Int. J. Heat Mass Transfer. 101, 69–75.

Chandraa, G.H., Kumar, J.N., Rao, N.M., Uthann, S., 2007. J. Crys. Grow. 306, 68–74.

Kumar, N., Sharma, V., Padha, N., Shah, N.M., Desai, M.S., Panchal, C.J., Protsenko, I.Yu., 2010. Cryst. Res. Technol. 45, 53–58.

Barreau, N., Marsillac, S., Bernède, J.C., Ben Nasrallah, T., Belgacem, S., 2001. Phys. Stat. Sol. (a) 184, 1, 179–186.

Tauc, J., Menth, A., 1972. J. Non. Cryst. Solids 8, 569–585.

Mariappan, R., Ragavendar, M., Gowrisankar, G., 2010. Chalcogenide Lett. 7, 211–216.

Ou, J.Z., Ge,W., Carey, B., Daeneke, T., Rotbart, A., Shan, W., Wang, Y., Fu, Z., Chrimes, A.F., Wlodarski, W., Russo, S.P., Xiang, Y., Kalantar-zadeh, K., 2015. ACS Nano. 9, 10313–10323.

Giberti, A., Gaiardo, A., Fabbri, B., Gherardi, S., Guidi, V., Malagù, C., Bellutti, P., Zonta, G., Casotti, D., Cruciani, G., 2016. Sens. Actuator B Chem. 223, 827–833.

Kergommeaux, A.D., Faure-Vincent, J., Pron, A., de Bettignies, R., Malaman, B., Reiss, P., 2012. J. Am. Chem. Soc. 134, 11659–11666.